Lab on a Chip

RSC Publishing

PAPER

View Article Online
View Journal

Microfluidic construction of minimalistic neuronal co-cultures†

Cite this: DOI: 10.1039/c3lc41224e

Ngoc-Duy Dinh,[a] Ya-Yu Chiang,[a] Heike Hardelauf,[a] Jenny Baumann,[a] Emily Jackson,[ab] Sarah Waide,[a] Julia Sisnaiske,[c] Jean-Philippe Frimat,[ad] Christoph van Thriel,[c] Dirk Janasek,[a] Jean-Michel Peyrin*[e] and Jonathan West*[af]

Received 5th November 2012,
Accepted 25th January 2013

DOI: 10.1039/c3lc41224e

www.rsc.org/loc

In this paper we present compartmentalized neuron arraying (CNA) microfluidic circuits for the preparation of neuronal networks using minimal cellular inputs (10–100-fold less than existing systems). The approach combines the benefits of microfluidics for precision single cell handling with biomaterial patterning for the long term maintenance of neuronal arrangements. A differential flow principle was used for cell metering and loading along linear arrays. An innovative water masking technique was developed for the inclusion of aligned biomaterial patterns within the microfluidic environment. For patterning primary neurons the technique involved the use of meniscus-pinning micropillars to align a water mask for plasma stencilling a poly-amine coating. The approach was extended for patterning the human SH-SY5Y neuroblastoma cell line using a poly(ethylene glycol) (PEG) back-fill and for dopaminergic LUHMES neuronal precursors by the further addition of a fibronectin coating. The patterning efficiency E_{patt} was >75% during lengthy in chip culture, with ~85% of the outgrowth channels occupied by neurites. Neurons were also cultured in next generation circuits which enable neurite guidance into all outgrowth channels for the formation of extensive inter-compartment networks. Fluidic isolation protocols were developed for the rapid and sustained treatment of the different cellular and sub-cellular compartments. In summary, this research demonstrates widely applicable microfluidic methods for the construction of compartmentalized brain models with single cell precision. These minimalistic *ex vivo* tissue constructs pave the way for high throughput experimentation to gain deeper insights into pathological processes such as Alzheimer and Parkinson Diseases, as well as neuronal development and function in health.

Introduction

Understanding the workings of the brain in healthy and diseased states remains a grand challenge. The brain is characteristically complex: it is highly compartmentalized, layered, and contains diverse cell types with plastic connectivity *via* axon and dendrite outgrowths. To better investigate the brain and the greater nervous system there is a need for more complex, yet well defined, neurobiology models which emulate the *in vivo* microenvironment. The interconnections within the brain are organized over micron length scales, dimensions which can be readily achieved using microfabrication techniques and replicated for high throughput analysis.

Patterning the cell adhesion microenvironment has been used to disentangle the connectivity of nervous tissue.[1] This capability has been applied to signal transmission[2–4] and growth dynamics[5] research, and recently used for high throughput neurotoxicity screening.[6–8] More complex spatially defined models can be fashioned using compartmentalized co-culture microenvironments. These microfabricated refinements of the Campenot chamber[9] contain microchannels for guided neurite outgrowth.[10] These tissue models can be used for studying pathology propagation following localized treatments with toxins, pathogens, mechanical damage or other insults and perturbations. Arrayed and disentangled neurite outgrowths provide a useful analytical display,[6–8] and the compartmentalized arrangement also brings the opportunity for selectively treating or isolating the soma or outgrowths for off-chip analysis.[11,12] These systems have been used to great effect to study axon degeneration and regeneration following

[a]Leibniz-Institut für Analytische Wissenschaften – ISAS – e.V., 44227 Dortmund, Germany. E-mail: J.J.West@soton.ac.uk
[b]Massachusetts Institute of Technology, Department of Chemical Engineering, Cambridge, USA
[c]Leibniz Research Centre for Working Environment and Human Factors at the University of Dortmund (IfADo), 44139 Dortmund, Germany
[d]BIOS – Lab on a Chip Group, MESA+, University of Twente, Enschede, The Netherlands
[e]CNRS, UMR 7102, Neurobiologie des Processus Adaptatifs, UPMC, Paris, France. E-mail: jmpeyrin@snv.jussieu.fr
[f]Institute for Life Sciences, University of Southampton, SO17 1BJ, UK
† Electronic supplementary information (ESI) available: See DOI: 10.1039/c3lc41224e

chemical[12,13] or laser[13–15] axotomy, tauopathy[16] and viral[17,18] dissemination, and mRNA localization in axons.[11] The systems have also been adapted for engineering the polarity of the synaptic junction using geometric diodes[19] or for synaptogenesis screening using HEK293 cells disguised as post-synaptic structures by recombinant decoration with neurolignin-1.[20]

Despite the many benefits of compartmentalized neuron culture platforms there is still great scope for improvement. Tens of thousands of neurons are currently seeded into each millimeter-scale compartment to attain significant numbers of inter-compartment connections.[11] Consequently, the neuron number, their positions and neurite interconnections are not controlled and the vast majority of the network is locally entangled. As a consequence only a small proportion of neurons (<5%) extend outgrowths between compartments. This limits the investigation of neurite-based (bio)material transport between the compartments and reduces the determinism of reconstructed neuronal networks. Moreover, extravagant cell usage (as with standard *in vitro* assays) is undesirable for high throughput experiments, especially with rare cells such as substantia nigra cells, dopaminergic cells suitable for Parkinson's research, or peripheral neurons. High throughput studies would require the sacrifice of multiple animals with data analysis complicated by inter-individual variance.

Microfluidic techniques are well suited for handling small cell numbers. Dynamic arraying methods can be used for metered cell loading with high spatial precision.[21–24] Unlike planar patterning methods, microfluidic arraying achieves reliable single cell registration. However, to maintain the spatial organization of cells arrayed using microfluidics it is necessary to provide a micropatterned cell adhesion environment which is aligned with the cell trapping structures. Microcontact printing of biomaterial patterns prior to enclosure within PDMS microchannels has previously been used.[25,26] However, progress with in chip biomaterial patterning is in its infancy, and is hampered by aggressive bonding conditions which damage biomaterials, the incompatibility of photoresists and processing conditions with biomolecules, and the requirement to align the biomaterial pattern with the microfluidic structures. This is especially problematic with elastomeric PDMS microstructures.

In this contribution we describe microfluidic circuits for single neuron arraying in combination with an innovative water masking process which enables *in situ* and aligned biomaterial patterning for directing outgrowths and maintaining the spatial precision of the neuronal networks. We have named these novel microfluidic circuits *Compartmentalized Neuron Arraying* (CNA) devices. These devices were used for arraying minimal neuronal inputs (10–100-fold less than existing systems) which formed precisely defined inter-compartment neuronal networks. Preparation of the in chip biomolecular patterns and the fluidic operations for neuron arraying and compartment-specific treatment are rapid, straightforward and completely accessible to neurobiologists.

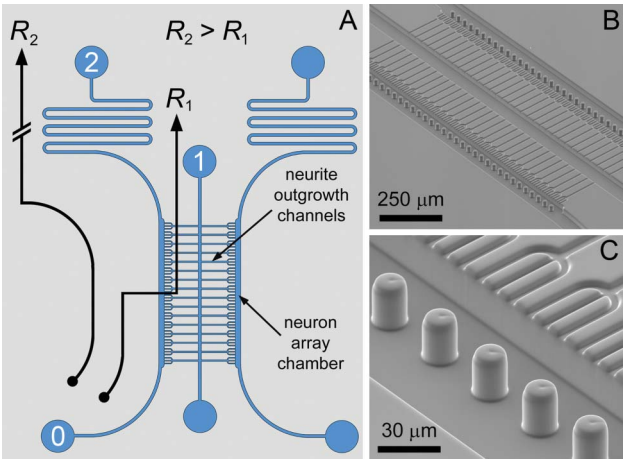

Fig. 1 The differential fluidic resistance circuit for single neuron arraying, with flanking culture chambers interconnected by neurite outgrowth channels (A). This schematic is not to scale. The actual device footprint is 15 × 15 mm. The path 0 → 1 connects the inlet channel *via* multiple neurite outgrowth channels to a central outlet channel. The paths have a lower fluidic resistance (R_1) than the serpentine path (0 → 2, R_2) for simultaneous neuron trapping along the linear arrays of cell traps in both compartments. SEM images of the bilayer compartmentalized neuron co-culture array with meniscus-pinning micropillars (B,C). Trident-shaped neuron trapping structures were used to promote fasciculation of the neurite outgrowths.

Concept

Microfluidic neuron arraying

Building on the microfluidic arraying method of Tan and Takeuchi[21] and the system developed in our laboratory for preparing arrays of contacting heterotypic single cell co-cultures[22] we have refolded the circuit for arraying neurons as two separated populations. The two neuron arraying compartments are coupled *via* microchannels that serve two functions; (i) flow paths for arraying single neurons, and (ii) for guiding neurite outgrowths to interconnect the two cell populations. The microfluidic circuit is illustrated in Fig. 1. Microfluidic arraying is based on the principle of differential fluidic resistance, with the majority of the flow along the path of least fluidic resistance and the minority along a higher fluidic resistance by-pass channel. The serpentine channel has a higher fluidic resistance than the neurite outgrowth channels ($R_2 > R_1$), producing a higher neurite outgrowth channel flow rate than the serpentine channel flow rate (*i.e.* $Q_1/Q_2 > 1$, eqn (1)):

$$Q/Q_2 = = \left(\frac{C_2(\alpha_2)}{C_1(\alpha_1)}\right)\cdot\left(\frac{L_2}{L_1}\right)\cdot\left(\frac{W_2+H}{W_1+H}\right)^2\cdot\left(\frac{W_1}{W_2}\right)^3 > 1 \qquad (1)$$

where W_1 is the aperture width, W_2 is the serpentine channel width, H is the channel height, L_1 is the neurite outgrowth channel length, L_2 is the length of the serpentine channel, and $C(\alpha)$ are constants defined by the aspect ratio ($0 < \alpha < 1$), and derived from the Darcy friction factor and the Reynolds number.[21,27] Single cells transported by the flow become individually trapped along the linear array of sub-cellular-sized

microstructured apertures and locally impede the flow, diverting subsequent neurons to the neighbouring apertures until all apertures are occupied by neurons. Complete occupancy switches the fluidic resistance ratio ($R_1 \gg R_2$) to divert the streamlines into the serpentine path ($0 \rightarrow 2$) to produce a by-pass mode of operation for the removal of excess neurons. In this fashion, the apertures define the number and position of the single neurons. Unlike our original co-culture system which required cellular valving (*i.e.* adhesion and flattening) before the addition of a second cell set,[22] the microfluidic neuron arraying circuit has a central channel which permits the simultaneous arraying of neurons in both flanking culture compartments. An alternative circuit was also developed which uses the same differential flow microarraying principle. In this device the central channel is removed necessitating sequential arraying (see ESI,† Fig. 1(A)), with a cellular valving interval as previously described[22] before arraying within the second compartment. This circuit prevents fluidic access to the synaptic compartment (*i.e.* the central channel), but importantly guarantees that the outgrowths remain linear for ease of tracing interconnections between individual cells within the networked co-cultured. By mirroring, the circuit was expanded to provide three neuron culture compartments for establishing two adjacent neuronal networks (see ESI,† Fig. 1(B)).

Materials and methods

Dimensions, fabrication and packaging

Bilayer devices were fabricated with a total height of ~25 μm. Trident structures were used for cell trapping to promote neuron-neuron contacts and enable fasciculation during neurite outgrowth. These also represent neurite outgrowth inlets which were 3-μm-wide and 3-μm-high. These are sufficiently small to act as cell filters, excluding nuclei and thus preventing neurons being transported into the neurite outgrowth channels during microfluidic arraying or migrating along these paths during culture. A trap pitch of 13 μm was used to accommodate the 12.0-μm-diameter SH-SY5Y cells and the slightly smaller primary neurons during microfluidic arraying. The neurite outgrowth channels intersected with the central channel (the axon interfacing channel) and connected the two flanking compartments over a distance of 500 μm. The circuit was designed with a differential flow ratio (Q_1/Q_2) of 1.5, requiring a serpentine channel length of 33 mm and width of 20 μm. An alternative system with the same flow ratio but without the central channel was also designed to ensure linear neurite outgrowth connectivity between the two cultures. The trident structures were replaced with 250-μm-long outgrowth channels. The CAD files for the compartmentalized neuron arraying (CNA) bilayer microfluidic circuits are available in the electronic supplementary information.

CNA devices were replicated in PDMS from bilayer SU-8 masters using previously published methods.[8,22] These were prepared using a first layer of SU-8 2 (Shipley) spin coated to a depth of 3.0 μm and patterned by photolithography. A second layer of SU-8 50 (Shipley) was spin coated to a depth of 20–25 μm. Major microfluidic paths (*i.e.* not the neurite outgrowth channels) aligned to those of the first layer were fabricated by a second photolithographic step. A CNA device was imaged by SEM (Quanta 200F (FEI)) and is shown in Fig. 1(A,B). A 3-mm-diameter biopsy punch (Kai Medical) was used to produce the inlet and outlet ports. Devices were either plasma bonded directly to a glass substrate or assembled by plasma bonding to a thin planar PDMS (Elastosil® RT 601, Wacker) layer supported by a ~170-μm-thick coverslip. Tygon™ tubing was used for convenience of plug and play operation for connection by simple insertion into the PDMS outlets. Cell arraying was achieved with an aspiration pump (N811KVP Mini Pump, KNF Neuberger, Laboport®, Germany) or with a syringe for manual aspiration (ESI†, Fig. 2).

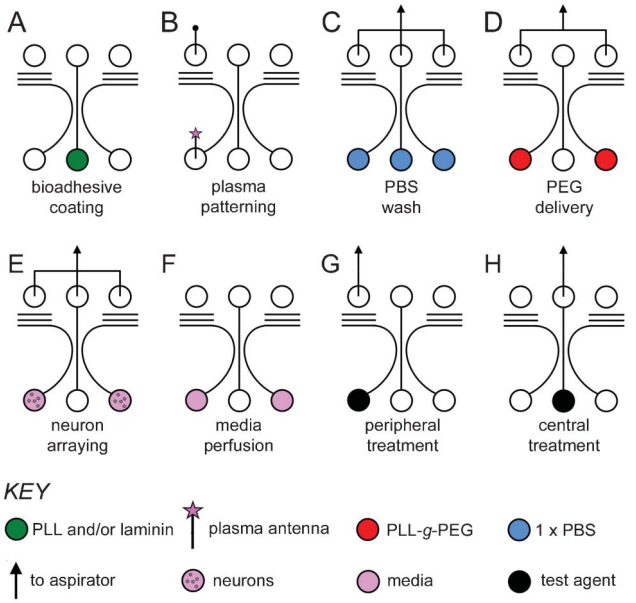

Fig. 2 Illustrated protocols for the different fluidic operations. PL and PLL-*g*-PEG patterning; addition of the cell adhesion layer (*e.g.* PL, green), with evaporation producing the aligned water mask (A), atmospheric air plasma treatment of the exposed PL (B). Two antenna pins are used, with the plasma introduction antenna illustrated with a pink star. PBS (blue) washing by aspiration is used to avoid contaminating the plasma-treated region with PL (C). Delivery of PLL-*g*-PEG (red) by aspiration to coat the plasma-treated regions (D). Cell loading; simultaneous microfluidic arraying of neurons to both flanking compartments by aspiration (E), media (pink) perfusion using a hydrostatic-driven flow (F). Isolated fluidic treatments; peripheral treatment of a test agent (black) delivered from the bottom flanking inlet by aspiration (G) and central treatment of a test agent delivered from the bottom central inlet by aspiration (H).

Water masking for *in situ* biomaterial patterning

A variety of neurons were used throughout this study to demonstrate the general applicability of the CNA devices and the biomaterial patterning approach. We have used mouse cortical neurons, readily available SH-SY5Y neuroblastoma cells and dopaminergic Lund human mesencephalic (LUHMES) cells, all of which have different adhesion biomolecule requirements. Methods for the preparation and culture of the different cell types are provided in the ESI.† For

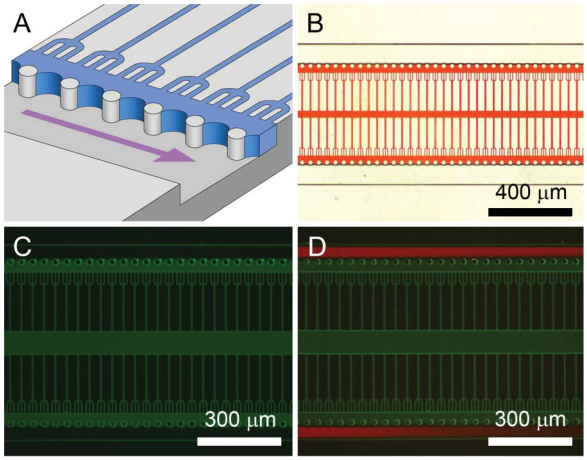

Fig. 3 Illustration of the water masking concept with the PDMS micropillars pinning the water meniscus in place for plasma stencilling (A). Curvature of the meniscus in the vertical plane has been neglected. Water mask visualized with a red dye and positioned by meniscus pinning (B). The patterned PL-FITC coating imaged after plasma stencilling (C). Addition of protein rejecting and cell repellent PLL-*g*-PEG-TRITC to a plasma-patterned PL-FITC coating (D). This was used for registration of the SH-SY5Y cells and also for patterning fibronectin coatings for the LUHMES cells.

primary neurons poly-amine (poly-lysine, PL; poly-ornithine, PO; or poly-ethyleneimine, PEI) coatings are required, and for LUHMES precursor neurons poly-ornithine (PO) with laminin or fibronectin is required. Our innovative biomaterial patterning method involves the use of water as a masking film during plasma patterning. The protocol for *in situ* water masking for biomaterial patterning is illustrated in Fig. 2(A–D), with results documented in Fig. 3. This process is as follows: Freshly plasma bonded devices were flooded with a 500 nL aliquot of poly-amine (poly-lysine, PL, either poly-D-lysine or poly-L-lysine, or poly-L-ornithine, PO, 100 μg mL^{-1} in PBS) into a central channel port by capillary action for coating of the PDMS surfaces. Evaporation from the large, 3-mm-diameter ports leads to the formation of a water mask (Fig. 3(A), with the aqueous solution remaining anchored to the meniscus-pinning structures, filling the neurite outgrowth channels and covering the neuron arraying sites (Fig. 3(B)). A time-lapse video of the water mask formation process is documented in the ESI† (Video 1). The water mask is established rapidly, requiring $\leqslant$5 min, and is inherently aligned to the neuron arraying sites and the neurite outgrowth channels. The pressure tolerance of the air–liquid interface scales inversely with the radius of curvature [$\Delta P = \gamma\,(1/R_h + 1/R_v)$], producing a highly stable interface at microfluidic dimensions. Nevertheless evaporation continues, reducing the lifetime of the water mask. To increase the lifetime to $\sim$15 min for ease of plasma patterning, 18 nL reservoir structures were positioned upstream of each culture compartment (ESI†, CAD files). These structures also act as convenient air traps during fluidic operation.

With the water mask in place the flanking microchannels are vacant, providing an air volume for the ignition of an atmospheric pressure plasma generated using a Tesla generator (VP23, Leybold-Heraeus, USA)[28,29] operating at 2 MHz, 30 kV signal. Stainless steel pins were inserted into the flanking inlet ports to act as antennas to aid plasma ignition within the flanking channels. Plasma treatment disintegrated the exposed poly-amine molecules, whereas molecules shielded by the water mask were protected. Disintegration of the exposed poly-amine layer was rapid, requiring $<$1 s to produce the biomaterial pattern. Excessive ($>$2 s) plasma treatments destabilised the water mask, disintegrating poly-amine-coated areas intended for neuron localization. A plasma-patterned PL coating is documented in Fig. 3(C). Plasma patterning was followed by a PBS wash by aspiration from the upper ports to remove the water mask and unbound poly-amine molecules (Fig. 2(C)). This fluidic operation prevents PL contaminating the plasma treated surfaces. Biomaterial patterning by plasma stencilling with a water mask is also applicable to the alternative microfluidic circuits that require cellular valving (see Fig. 1(A) and 1(B)). With these circuits, the poly-amine coatings are washed with PBS prior to water masking. This removes unbound biomolecules to prevent contamination of the plasma-treated PDMS surface during removal of the water mask.

The polyamine-PDMS patterns are suitable for primary neuron patterning. For SH-SY5Y and LUHMES cells the plasma-treated regions were PEGylated using 10 μL of the graft co-polymer poly-L-lysine-poly(ethylene glycol) (PLL-*g*-PEG in PBS, 100 μg mL^{-1}, Surface Solutions, Switzerland) added to the bottom flanking inlets and introduced by aspiration for 5 min. Without interrupting the flow, excess PLL-*g*-PEG was removed by exchange with a PBS buffer (see Fig. 3(D)). The PEGylated regions prevent the adhesion of SH-SY5Y cells. For the culture and maintained differentiation of LUHMES cells, the CNA device was further treated with a fibronectin (100 μg mL^{-1}, Sigma-Aldrich) solution. The PEGylated regions reject protein adsorption, with the fibronectin co-localizing with the patterned PL or poly-ornithine coating. Neuron patterns were characterized using a patterning efficiency term E_{patt}, defined as the number of cells adhering to the plasma activated area N_p relative to the number of cells adhering to an equivalent sized, untreated area N_u, calculated using the following expression:[30]

$$E_{patt} = 2 \times \left(\frac{N_p}{N_p + N_u} - \frac{1}{2} \right) \times 100. \qquad (2)$$

Using this equation, perfectly patterned cells have an E_{patt} of 100%, cells randomly adhering to the surface have a value of 0% and patterns of cells perfectly excluded from the activated area have a value of −100%.

Microfluidic arraying, immunostaining and fluidic isolation

Prior to cell loading CNA devices were primed with media using an aspiration pump (N811KVP Mini Pump, KNF Neuberger, Laboport®, Germany). A 20 μL cell suspension (1–2 × 10^6 cells mL^{-1}) was dispensed into the flanking inlet ports (0, in Fig. 1) and the upper 3 outlets were connected by equal-length tubing *via* a 4-way union (see ESI,† Fig. 2) to either an aspiration pump or a syringe for gentle manual aspiration.

Complete arraying required <30 s. Once the different arrays were fully populated with neurons, the circuit diverts the flow to the serpentine path such that excess cells exit. The CNA devices were disconnected, the inlet ports were filled with media and the devices were placed in the incubator for cell culture. Media exchange was achieved by periodic media perfusion using hydrostatic feed (1–2 mm column height difference), or by simply submerging the CNA devices in media. The protocols for cell loading and media perfusion are illustrated in Fig. 2(E) and 2(F).

Compartmentalized neuron cultures were periodically imaged using a phase contrast inverted microscope (Olympus IX81 or a Zeiss Axiovert 200 M) and fluorescently visualized using DAPI-stained DNA, and β(III)-tubulin immunocytochemical staining. This involved the addition of reagents using a hydrostatic-driven liquid feed using a 3 mm port height difference. The media was replaced with a PBS wash buffer for 10 min and the cells were then fixed using neutral buffered 4% formaldehyde (SAV, Liquid Production, Germany) for 30 min at 37 °C. Non-specific binding was blocked using a triple filtered (200 nm pore Ø) solution of 5% milk/PBS for 1 h at room temperature, followed by a 20 min PBS rinse and then incubation with a 1 : 2000 dilution of rabbit-anti-β(III)-tubulin primary antibody (Covance) in PBS containing 0.1% Triton-X for 3 h at 37 °C. This was followed by a 10 min PBS wash prior to a 1.5 h incubation at 37 °C with a 1 : 300 dilution of Cy2-labeled donkey-anti-rabbit secondary antibody (Dianova) in PBS containing 300 nM DAPI (Invitrogen). Short, ~5 min PBS washes were used to reduce non-specific binding prior to fluorescent imaging.

Hydrostatic-driven flow and aspiration-driven flow methods were investigated to identify optimum conditions for selective treatment of the central compartment or the flanking compartments. Hydrostatic-driven flow requires pressures to be precisely balanced, necessitating flows in the three main channels, each driven by a 3 mm column elevation in the upper, outlet ports. The aspiration method entailed filling all ports equally, with flow from bottom to top driven by a syringe pump (PHD 2000, Harvard Apparatus) interfaced to the microfluidic device *via* Tygon™ tubing. The flow assigned for treatment was doped using 10 μM FITC (see Fig. 2(G) and 2(H)) for fluorescent imaging. Images were analysed using ImageJ with data normalized relative to the maximum value for each experimental series.

Fluidic isolation using a hydrostatic-driven flow was also evaluated by simulation. The CFD flow module of SolidWorks (Dassault Systèmes SolidWorks Corp., MA, USA) was used to map the pressure and velocity distributions within the CNA microfluidic circuit. The time-dependent laminar state was described by solving the Navier–Stokes equations using the properties of water, zero surface roughness, a no-slip boundary condition and ambient temperature and pressure being 293.2 K and 101 325 Pa, respectively. Glass was chosen as a proxy material for the hydrophilic surfaces; plasma treated PDMS, with or without poly-amine of PLL-*g*-PEG coatings. A 101 374 Pa pressure was assigned to the top three ports and 101 344.6 Pa to the bottom three (*i.e.* equivalent to a 3 mm column height difference). The fluidic circuit was discretized into >3.5 million whole or partial fluid cells, with a simulation entailing 376 iterations.

Results and discussion

Water masking for aligned in chip biomolecule patterning

To maintain neuron arrangements throughout lengthy experimental timescales it is necessary to pattern the adhesive microenvironment. Great progress has been made with biomaterial patterning on planar substrates to spatially define cell cultures.[6–8,31–35] However, methods for aligned biomaterial patterning within microfluidic environments are poorly developed. The described CNA devices require biomaterial coatings on the neurons trapping sites to register the neurons. In addition, the outgrowth channels require coating to promote neurite guidance between the culture compartments. To meet this requirement we have developed a novel water masking technique for patterning biomaterials *in situ*, after device bonding, with meniscus-pinning microstructures used to align the patterning process: Freshly plasma bonded PDMS devices are highly hydrophilic enabling the device to be flooded with a small poly-amine volume (500 nL) by capillary action. Plasma activation produces silanol-rich PDMS surfaces, well suited for the electrostatic assembly of poly-amine coatings. The silanol-rich, hydrophilic PDMS surface quality decays as hydrophobic PDMS oligomers diffuse to the surface in a matter of 10's of minutes. It is therefore recommended that the poly-amine coating be added directly following plasma bonding. For convenience of operation in a biology laboratory a handheld Tesla generator or corona discharge system can be used for both plasma bonding and subsequent biomaterial patterning. The poly-amine solution also serves as the water mask, which becomes anchored to the meniscus-pinning micropillars, protecting the poly-amine coating on the neuron arraying sites and within the neurite outgrowth channels. The water mask is established rapidly (⩽5 min) by evaporation and, by virtue of the upstream reservoir structures, remains intact for ~15 min, a manageable window for plasma stencilling which requires <1 s to treat each compartment. This brief plasma treatment disintegrates the exposed poly-amine coating to produce a PDMS-biomaterial pattern. PDMS prevents the adhesion of primary neurons, making poly-amine patterning by water masking effective for establishing primary neuron patterns.

The SH-SY5Y human neuroblastoma cell line was readily available and preferred for optimizing the microfluidic neuron arraying and culturing conditions. However, these cells can adhere to plasma-activated PDMS.[30] To mimic the cell patterning characteristics of primary neurons with the SH-SY5Y line a cell repellent material coating was required. PEGylated surfaces resist SH-SY5Y cell adhesion.[8] In a preliminary experiment using PL/PLL-*g*-PEG patterns on planar glass substrates differentiated SH-SY5Y cells had a patterning efficiency of 87% after 5 DIV culture (ESI†, Fig. 3). To achieve material co-patterning within the microfluidic device, PL was first plasma patterned by water masking as before and then a PLL-*g*-PEG backfill was used (Fig. 3(D)). For

details please refer to the *Water Masking for In Situ Biomaterial Patterning* section in the Materials and Methods. The protocol for biomaterial patterning is also illustrated in Fig. 2(A–D). The use of PEGylated regions allows proteins to be subsequently added which is preferred to the application of a PL-protein mixture. For example, fibronectin can be added for the differentiation and maintenance of LUHMES cells[36] and laminin for promoting outgrowths from primary cultures.[37] The novel water masking method for *in situ* biomaterial patterning by plasma stencilling is simple, reliable and widely applicable to the variety of adhesion materials appropriate to the different neuron types. With the minimal expense of a handheld plasma source[28,29] the method is suitable for adoption within neurobiology laboratories.

Microfluidic arraying with single neuron precision

The differential resistance fluidic circuit was used to prepare neuron arrays with single cell precision. A video of the process is provided in the ESI, † Video 2. The fluidic circuit produces multiple streamlines, with many narrow streamlines each exiting *via* a neurite outgrowth channel and other streamlines continuing to the serpentine channel. The majority of the streamlines converge at the arraying site, producing tightly packed and sub-cellular-sized transport paths, such that the first cell is generally loaded in the trap furthest from the inlet where only a single streamline remains. Upon cell trapping the streamline is removed such that subsequent cells are sequentially trapped. In this manner neuron arrays can be prepared with single cell precision. Choice examples of arrayed SH-SY5Y and LUHMES cells are documented in Fig. 4, with the larger, original images documented in ESI,† Fig. 4. Mouse primary neurons were also arrayed with single cell precision. Arraying is rapid, with ~100 neurons arrayed in each culture chamber in ~10 s. This corresponds to an input of <1000 cells. Cells remaining in the inlet can be retrieved for experiment parallelization using multiple CNA devices.

Microfluidic arraying imposes fluidic stress for a short duration. In contrast, subjecting cells to small but lengthy mechanical strain causes cell deformation which can lead to cell death. An example of this effect resulting from slow arraying using gravity feed for 30 min is documented in the ESI,† Fig. 5. Likewise, direct trapping at microscale orifices (without using differential microflows) causes extreme cell body deformation, again leading to cell death. These systems are unsuitable for neuron culture but can be put to good effect for short-term single cell electrophysiology.[38]

The CNA system effectively achieves single neuron arraying, with ~1 neuron per trap arrayed in both the neuron culture compartments. Arraying of neuron doublets or large neurons can however perturb the densely packed parallel streamlines which leads to occasional vacancies in the array, deviation from the arraying sequence and a slight increase in the neuron : trap ratio. In a triplicate experiment compartments each with a 99-trap array (33 tridents) were reproducibly loaded; 1.14 (SD ± 0.09) SH-SY5Y neurons/trap, with 95.0% (SD ± 1.3%) traps occupied and 73.7% (SD ± 6.6%) cells occupying a single trap (see Table 1 and Fig. 4(A–C)). Similar results were obtained when arraying mouse cortical neurons and LUHMES cells (see Fig. 4(D)). The microfluidic arraying

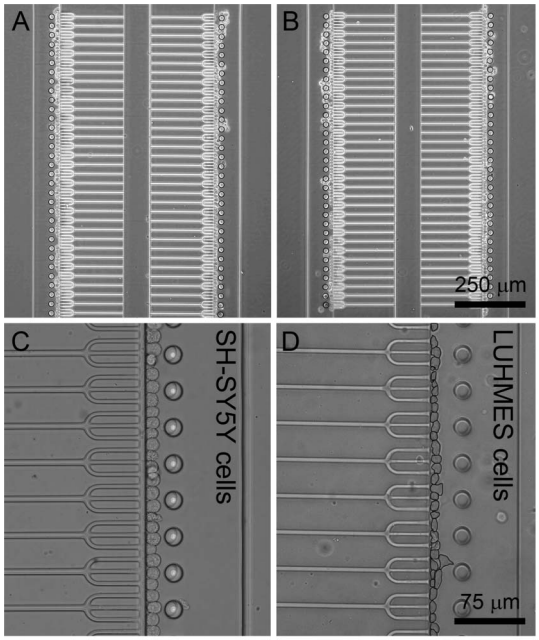

Fig. 4 Images from repeat experiments (A,B) of fully arrayed differentiated SH-SY5Y neuron-like cells in the CNA device. The meniscus-pinning micropillars have been outlined to distinguish these from the single neurons. Higher magnification image of optimally arrayed SH-SY5Y cells (C) and LUHMES cells (D) imaged 4 h after arraying. The LUHMES cells are outlined to aid visualization. The larger, original images are available in the ESI, † Fig. 4.

method efficiently transported cells to the traps, with excess cells diverted from the culture site leaving only 4.3% (SD ± 2.3%) of cells remaining off-site (*i.e.* on the PEG-coated region). The low off-site numbers are a feature of the efficiency of the microfluidic arraying principle and also the anti-fouling quality of the PLL-*g*-PEG adlayer.

The neurite outgrowth inlets were 3 μm wide and high, suitably small to exclude neurons while being permissive for neurite outgrowth. A trap pitch of 13 μm was used to accommodate the 12.0-μm-diameter SH-SY5Y cells and the slightly smaller mouse cortical neurons and LUHMES cells. HEK293 cells are appropriate for synaptogenesis studies,[20] but have a significantly larger suspension diameter of 16.2 μm (SD ± 2.1). The arraying quality with HEK293 cells was markedly reduced, with only 38.8% of cells occupying single traps. A trap pitch greater than the cell suspension diameter is therefore required for precision single neuron arraying. A more detailed comparison of the effect of cell type and size on arraying quality is documented in Table 1.

With appropriate dimensions differential flow single cell arraying has high precision. However, with the current CNA devices not all neurons are arrayed. The microfluidic circuit generates parallel streamlines such that neurons arriving in outer parts of the flow continue to the serpentine channel. As a consequence a number of cells are wasted. Nevertheless the presented device is 10–100-fold more economical with cell material than other compartmentalized systems.[10–20,39] This also highlights the advantage of using aspiration for cell arraying, a process which can readily manage minimal cell

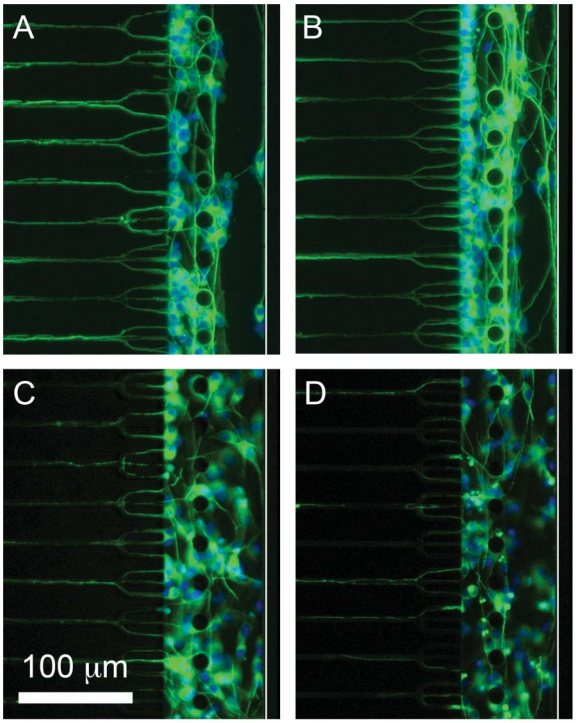

Fig. 5 *In situ* neuron patterning. Differentiated human SH-SY5Y neurons cultured for 5 days within the CNA devices on a PL/PLL-*g*-PEG pattern (A,B) and on a continuous PL coating (C,D). Biomaterial patterning increases neurite guidance into the outgrowth microchannels.

suspension volumes (*e.g.* 1 μL). Should absolute economy with cell material be necessary, deterministic lateral displacement[40] structures can be positioned upstream for deflecting all neurons into the arraying streamlines. Such sparing use of cells affords the possibility to undertake high throughput research using neurons from a single animal.

In chip patterned culture of neuronal networks

The arrayed neurons remain registered to the biomaterial adhesion pattern during lengthy in chip culture. With a continuous, unpatterned poly-lysine coating excessive numbers of neurons adhered upstream requiring several minutes to deliver sufficient neuron numbers for adequate arraying. In addition, those positioned at the trident inlets later migrated to take on a dispersed distribution: The E_{patt} of SH-SY5Y cells cultured on an unpatterned, continuous PL coating for 6 days was 1.7% (*i.e.* randomly positioned, see eqn (2)). In comparison, the E_{patt} of SH-SY5Y cells cultured on a PL/PLL-*g*-PEG co-material pattern for 6 days was 76.8%. Although differentiated these cells continue to divide, albeit at slow rates, increasing the cell number 2–3-fold in these experiments. Nevertheless the PL/PLL-*g*-PEG pattern acts to retain neurons and their progeny at the array site. In comparison, non-dividing mouse cortical neurons were registered selectively to the poly-lysine pattern with an E_{patt} of 89.5% during culture for 6 days. In a similar experiment, the E_{patt} of LUHMES cells cultured on a fibronectin and poly-L-ornithine/PLL-*g*-PEG pattern, was 75.5% whereas the E_{patt} was 1.1% on an unpatterned poly-L-ornithine and fibronectin coating. Images of the different in chip patterned and non-patterned SH-SY5Y cultures are shown in Fig. 5. However, plasma-mediated disintegration of the PL coating is not always complete, with fluorescence from PL-FITC observed on the microchannel wall opposite from the trapping sites (ESI,† Fig. 6). Here occasional cells adhered and became localised (Fig. 5(A) and 5(B)).

Extensive neurite outgrowths developed from neurons patterned within the CNA system. These entered and extended within ~90% of the neurite outgrowth channels. On the continuous, unpatterned PL coating outgrowth quality varied from region to region, overall producing outgrowth levels of ~70% (Fig. 5(C) and 5(D)). This evidence indicates that the PL/PLL-*g*-PEG pattern acts to promote neurite extension into the outgrowth channels. In addition, cell body deformation and probable cell death was evident in a number of regions on the continuous PL coating. We attribute this to mechanical stresses exerted during the prolonged timescales (>10 min) required to array neurons on a continuous PL coating. Biomaterial patterning therefore serves two roles; (i) ease of rapid, low stress arraying and (ii) guidance of outgrowths into the neurite channels. The neurite outgrowths had an affinity for PL-coated topographical cues within the microstructured environment. This promotes extension into the neurite outgrowth channels and also an encircling-type interaction[41] with the meniscus pinning pillars which define the PL/PLL-*g*-PEG boundary (Fig. 5(A) and 5(B)).

To date, we have cultured LUHMES cells in CNA devices on patterned poly-ornithine with fibronectin surrounded by a PLL-*g*-PEG adlayer for 7 days, SH-SY5Y cells on a poly-L-lysine/PLL-*g*-PEG co-material pattern and mouse cortical cultures on a patterned poly-L-lysine coating for 13 days. Together these results provide evidence that microfluidic arraying and in chip patterned culture is feasible for a variety of neuron types, their required adhesion materials and typical experimental timescales.

Table 1 Comparison of microfluidic arraying results from a triplicate experiment with SH-SY5Y cells along with results from experiments using LUHMES and HEK293 cell types, and a duplicate experiment with mouse cortical neurons. The CNA devices contained 198 trapping sites, or 99 in each culture compartment (mean values are presented with ± denoting standard deviation)

Cell type	Suspension diameter	Cell number arrayed	Cells/trap	Cells on single traps	Cells on ⩾2 traps	Cells on pillars	Cells off-site
SH-SY5Y	12.0 ±1.2 μm	231 ±23	1.14 ±0.09	73.7 ±6.6%	4.9 ±0.9%	17.1 ±2.8%	4.3 ±2.3%
Mouse cortical	~10 μm	218	1.10	71%	ND	23%	6%
LUHMES	10.7 ±1.8 μm	223	1.13	73.1%	3.1%	15.3%	8.5%
HEK293	16.2 ±2.1 μm	188	0.95	38.8%	20.7%	37.8%	2.7%

Arrayed neurons developed outgrowths that extended between the CNA compartments. Cortical neuron axon outgrowths spanning both culture compartments were established in 7 days. Human SH-SY5Y cells required 4–6 days to develop inter-compartment outgrowths. The majority (85.3% (SD ± 5.5%)) of the outgrowth channels contained neurites from one or more neurons which extended between the two culture compartments. This demonstrates the feasibility of using minimal neuron numbers to establish highly networked compartmentalized co-cultures. The absence of guidance in the central channel led to deviation from the otherwise linear neurite outgrowth geometry. Extreme examples of this effect are documented in ESI,† Fig. 7, and highlight the difficulty of mapping individual inter-compartment neurite paths.

With applications that do not require access to the axon and dendrite sub-cellular compartment this problem can be managed by removing the central channel from the microfluidic circuit to guarantee linear outgrowths between the culture compartments (ESI,† Fig. 1(A)). This approach requires sequential cell arraying entailing an interval (typically 4 h) necessary for the first cell population to adhere and become flattened (*i.e.* cellular valving).[22] In a further design iteration, the central channel can also serve as another culture compartment for other neurons, oligodendrocytes and other heterotypic combinations (ESI, † Fig. 1(B)). Cells can be arrayed in the central compartment, followed by cellular valving in readiness for cell arraying in the flanking compartments (the arraying sequence can also be reversed). Cultured within these circuits, the neurite outgrowths remain linear and develop to establish inter-compartment networks. Network levels, defined as the percentage of channels with continuous β(III)-tubulin staining of neurite structures between both compartments, were 100% for both the two- and three-compartment neuronal network systems (Fig. 6(A) and 6(B)). Again, this provides a clear demonstration that fully networked neuronal co-cultures can be established using minimal cell inputs. Although primary neurons do not replicate, their superior neurite outgrowth levels lend weight to our prediction that they will also develop perfect inter-compartment network levels.

Considering the single cell handling capability of microfluidics it is tempting to envisage neuronal co-cultures engineered with single neuron to single neuron connectivity. However, neurons have a natural affinity for one another, organising into clusters with cell-cell contacts promoting the development of outgrowths (see Fig. 5(A) and 5(B)). For example, isolated single SH-SY5Y neuroblastoma cells do not ordinarily produce outgrowths.[6,8] This highlights a general lesson in that we often need to refine our engineering perspectives to best mimic neuronal tissues *in vitro.* To balance these interests an array system comprising isolated multi-neuron adhesion nodes is recommended. The neuron adhesion strip in the current system can be interrupted to define an array of individual nodes by adjoining the meniscus-pinning pillars to either side of the trident inlets. The meniscus-pinning structures are therefore no longer free-standing which should greatly limit local entanglement and enable interactions, from node to node, to be tracked along neurites of defined length. This neuronal node isolation approach could also be used to improve synaptogenesis arrays[20] and could further be used to efficiently interface networked neuronal populations with microelectrode arrays.[42–45] Such an arrangement can be used to validate the morphological connectivity of the network and, more importantly, the functional capacity of the neuronal network.

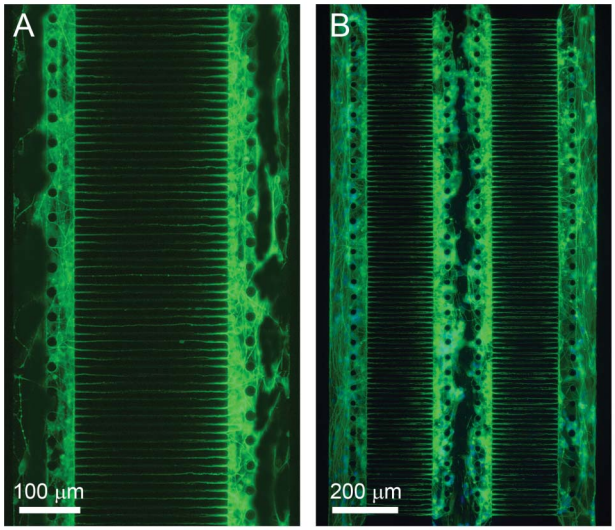

Fig. 6 Highly interconnected SH-SY5Y co-cultures in 2-compartment (A) and 3-compartment (B) CNA systems. In the 3-compartment experiment, a patterned PL surface was only provided in the central compartment; a continuous PL coating was used in the flanking compartments. Neurons and neurite outgrowths were immunostained for *β*(III)-tubulin following culture for 5 days.

Compartment-specific microfluidic treatments

A great strength of compartmentalized neuronal co-culture systems is the ability to selectively treat cell or outgrowth compartments,[11,39] making fluidic isolation in the CNA systems a pre-requisite for general applicability. Although apparently trivial, this requires pressures and flow rates to be precisely balanced throughout the period of treatment. Microfluidic compartmentalized neuronal co-cultures are highly sensitive to even the smallest pressure differences. This is especially true of the CNA circuits. Addition of a test substance into one channel introduces convection paths throughout the device, thereby exposing all compartments. To ameliorate this problem, parallel top to bottom pressure-driven flows (*i.e.* the reverse direction to neuron arraying) through the three main paths can be used to minimise the pressure drop across the neurite outgrowth channels (ESI,† Fig. 8(A)). Nevertheless the lower fluidic resistance of the central channel generates outward flow (ESI,† Fig. 8(B)) such that attempts to selectively treat the central channel result in contamination of the flanking, culture channels within a matter of minutes (Fig. 7(A) and ESI,† Fig. 9(A)). Hydrostatic driven flow (HDF) can, however, be used to selectively treat the flanking channels (Fig. 7(B)). Contamination of other regions of the device does not occur even during HDF for 24 h (ESI,† Fig. 9(B)). Instead, the minor outward flow acts to dilute the treatment. However, the fluidic resistance imposed by the

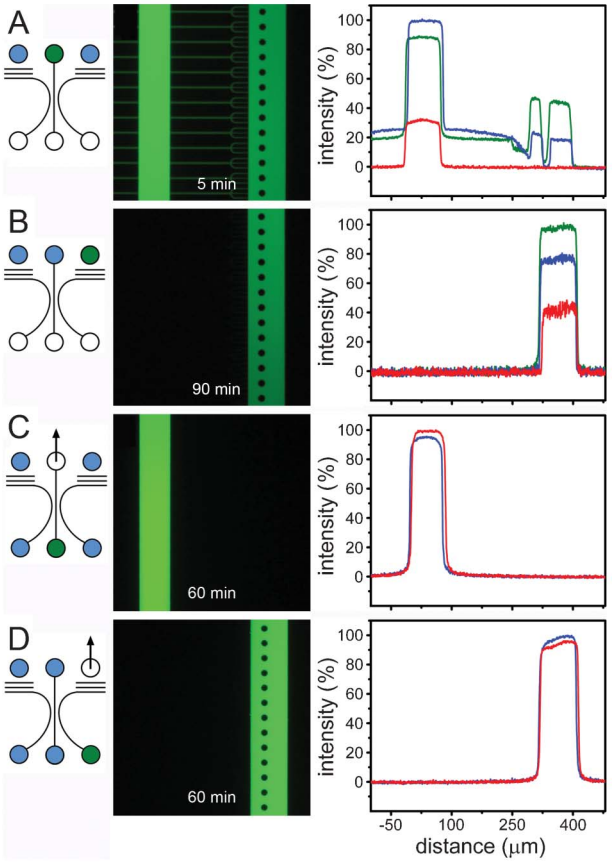

Fig. 7 Comparison of fluidic isolation using hydrostatic-driven (A,B) and aspiration-driven (C,D) flows. Hydrostatic-driven flow (HDF) involved filling the upper 3 ports, one with test agent (green) the others with PBS (blue), with a 3 mm column elevation relative to the bottom ports. The pressure difference generates outward flows through the neurite outgrowth channels which progressively contaminates the culture compartments (A). Images were recorded at 30 s (red line), 1 min (blue line) and 5 min (green line) intervals. The micropillars exclude the fluorescent volume. HDF treatment of the flanking, culture compartment was slow. Concentration rise at 40 min (red line), 60 min (blue line) and the maximum at 90 min, (green line, B). Aspiration-driven selective treatments are illustrated with an arrow and can be used for the rapid and selective treatment of the central (C) and flanking compartments (D). Treatments were established in 1 min (red lines) and were maintained for the duration of the experiment; 60 min (blue lines).

serpentine channels result in lengthy periods (>60 min) required to establish full concentration treatment of the flanking channels.

Aspiration is more straightforward and can be used for the rapid (~1 min) and maintained selective treatment of the central channel or the flanking channels (Fig. 7(C) and 7(D)). Differential flow operation is prevented by connecting an aspiration device to a single upper outlet. Test substances can be drawn from the bottom ports, with the high fluidic resistance neurite outgrowth channels acting to effectively isolate the treatment. For central or flanking treatments, the flow through the neurite outgrowth channels produces only minimal dilution of the test substance and ensures zero contamination of other compartments. Importantly, the two- and three-compartment systems (*i.e.* those lacking a central fluid delivery channel) are based on the same microfluidic circuit principles and can also be used with aspiration-based fluid-drive for selective treatment of the different culture compartments.

Outlook and applications

PDMS-based devices and especially the water masking technique for biomaterial pattern are far from ideal for manufacture. Concerns are also raised over the stability of biomolecular patterns during storage and transport. Instead, device replication, biomaterial patterning and fluidic operation are intended for the neuroscientist end-users. Indeed, CNA devices have already been used for biomaterial patterning and neuron arraying by neuroscientists in their laboratories.

In the present study we have established compartmentalised homotypic neuronal co-cultures and demonstrated the feasibility of arraying HEK293 cells which can be used with neurons in a heterotypic co-culture to provide arrays of artificial synapses.[20] The CNA circuits can be used to establish many other heterotypic co-cultures to model different neurobiological interactions, such as the neuromuscular junction, the role of glial cells during axon myelination,[46–48] immune cell scenarios implicated in autoimmunity-based neurodegeneration and spatially defined cues for neuronal stem cell differentiation. In addition, the compartmentalized nature of the co-culture systems enable investigations into the propagation of materials and pathological responses with notable examples being amyloid trafficking,[49] toxin dissemination, especially nanoparticulates such as manganese, and the distribution of virus and prion infectious agents. The compartmentalised systems also provide a spatially standardized imaging display for network integrity measurements and functional assays employing fluorescent Ca^{2+} reporters. Beyond this, precision cell positioning can be used to reliably interface neurons and outgrowths with microelectrodes for investigating neuronal network electrophysiology. Lastly, optofluidic interfacing can be considered: Microfluidic delivery in combination with pulsed laser uncaging[50] can be used to deliver neurotransmitter signals with the desired frequencies necessary to investigate the neurotransmitter basis of long term potentiation and depression[51] underlying memory formation. In summary, the described CNA circuits are highly versatile and can be used to tackle a huge variety of neuroscience questions.

Conclusions

Microfluidic circuits based on differential flow principles have been developed for arraying neurons within interconnected compartments with single cell precision. In addition, a novel *in situ* patterning technique involving plasma stencilling with water masking has been established and used for the aligned patterning of adhesion biomaterials within the microfluidic device. The biomaterial pattern promotes neurite outgrowth guidance and maintains the spatial organization of the neuronal network. The materials and methodologies are generally applicable to the variety of neuron types and require

only minimal cellular inputs. In addition, methods for effective fluidic isolation are described and can be used for localised chemical or biological perturbation of networked neuronal co-cultures. The user friendly construction and operation principles are readily accessible to the neuroscience community. These capabilities bring the opportunity to investigate neuronal interactions and disease states with high spatial resolution in a manner which is amenable to high throughput experimentation using cells harvested from a single animal.

Acknowledgements

The authors are grateful to Ulrich Marggraf (ISAS) for SU-8 fabrication, Maria Becker (ISAS) for SEM imaging, Nicole Schöbel (IfADo) for neurobiology discussions and Vanessa Hausherr (IfADo) for immunostaining advice. The LUHMES cells used in this research were a kind gift from Marcel Leist (Universität Konstanz). The research was financially supported by the Deutsche Forschungsgemeinschaft (DFG WE3737/3-1), a Bundesministerium für Bildung und Forschung grant (BMBF 0101-31P6541) and by the Ministerium für Innovation, Wissenschaft und Forschung des Landes Nordrhein-Westfalen. Heike Hardelauf thanks the International Leibniz Graduate School ''Systems Biology Lab-on-a-Chip'' for financial support. JMP was funded by ANR "PrionTraf", "Prion SensiTNF" and "Fondation de France''.

References

1 D. Kleinfeld, K. H. Kahler and P. E. Hockberger, *J. Neurosci.*, 1988, **8**(11), 4098–4120.
2 M. S. Ravenscroft, K. E. Bateman, K. M. Shaffer, H. M. Schessler, D. R. Jung, T. W. Schneider, C. B. Montgomery, T. L. Custer, A. E. Schaffner, Q. Y. Liu, Y. X. Li, J. L. Barker and J. J. Hickman, *J. Am. Chem. Soc.*, 1998, **120**(47), 12169–12177.
3 A. K. Vogt, G. Wrobel, W. Meyer, W. Knoll and A. Offenhäusser, *Biomaterials*, 2005, **26**, 2549–2557.
4 F. Patolsky, B. P. Timko, G. Yu, Y. Fang, A. B. Greytak, G. Zheng and C. M. Lieber, *Science*, 2006, **313**, 1100–1104.
5 Z. D. Wissner-Gross, M. A. Scott, D. Ku, P. Ramaswamy and M. F. Yanik, *Int. Bio.*, 2011, **3**, 65–74.
6 J.-P. Frimat, J. Sisnaiske, S. Subbiah, H. Menne, P. Godoy, P. Lampen, M. Leist, J. Franzke, J. G. Hengstler, C. van Thriel and J. West, *Lab Chip*, 2010, **10**, 701–709.
7 J. West, J.-P. Frimat, J. Sisnaiske, C. van Thriel and J. G. Hengstler, DE 10 2009 021 876.9, PCT/EP2010/002811, EP 09 012 960.2.7 and US 2012-0065102A1.
8 H. Hardelauf, J. Sisnaiske, A. Ali Taghipour-Anvari, P. Jacob, E. Drabiniok, U. Marggraf, J.-P. Frimat, J. G. Hengstler, A. Neyer, C. van Thriel and J. West, *Lab Chip*, 2011, **11**, 2763–2771.
9 R. B. Campenot, *Dev. Biol.*, 1982, **93**(1), 1–12.
10 A. M. Taylor, S. W. Rhee, C. H. Tu, D. H. Cribbs, C. W. Cotman and N. L. Jeon, *Langmuir*, 2003, **19**, 1551–1556.
11 A. M. Taylor, M. Blurton-Jones, S. W. Rhee, D. H. Cribbs, C. W. Cotman and N. L. Jeon, *Nat. Methods*, 2005, **2**(8), 599–565.
12 D. Kilinc, J.-P. Peyrin, V. Soubeyre, S. Magnifico, S. Laure, J.-L. Viovy and B. Brugg, *Neurotoxic. Res.*, 2011, **19**, 149–161.
13 L. Li, L. Ren, J. C. Wang, Y. Wang, Q. Tu, J. Xu, R. Liu, Y. Zhang, M. S. Yuan, T. Li and J. Wang, *Anal. Chem.*, 2012, **84**(15), 6444–6453.
14 Y. T. Kim, K. Karthikeyan, S. Chirvi and D. P. Dave, *Lab Chip*, 2009, **9**, 2576–2581.
15 A. N. Hellman, B. Vahidi, H. J. Kim, W. Mismar, O. Steward, N. L. Jeon and V. Venugopalan, *Lab Chip*, 2010, **10**(16), 2083–2092.
16 A. Kunze, R. Meissner, S. Brando and P. Renaud, *Biotechnol. Bioeng.*, 2011, **108**(9), 2241–2245.
17 W. W. Liu, J. Goodhouse, N. L. Jeon and L. W. Enquist, *PLoS One*, 2008, **3**(6), e2382.
18 A. Markus, S. Grigoryan, A. Sloutskin, M. B. Yee, H. Zhu, I. H. Yang, N. V. Thakor, R. Sarid, P. R. Kinchington and R. S. Goldstein, *J. Virol.*, 2011, **85**(13), 6220–6233.
19 J.-M. Peyrin, B. Deleglise, L. Saias, M. Vignes, P. Gougis, S. Magnifico, S. Betuing, M. Pietri, J. Caboche, P. Vanhoutte, J.-L. Viovy and B. Brugg, *Lab Chip*, 2011, **11**(21), 3663–3673.
20 P. Shi, M. A. Scott, B. Ghosh, D. P. Wan, Z. Wissner-Gross, R. Mazitschek, S. J. Haggarty and M. F. Yanik, *Nat. Commun.*, 2011, **2**, 510.
21 W.-H. Tan and S. Takeuchi, *Proc. Natl. Acad. Sci. U. S. A.*, 2007, **104**(4), 1146–1151.
22 J.-P. Frimat, M. Becker, Y.-Y. Chiang, D. Janasek, J. G. Hengstler, J. Franzke and J. West, *Lab Chip*, 2011, **11**(2), 231–237.
23 D. Di Carlo, N. Aghdam and L. P. Lee, *Anal. Chem.*, 2006, **78**(14), 4925–4930.
24 D. Di Carlo, L. Y. Wu and L. P. Lee, *Lab Chip*, 2006, **6**(11), 1445–1449.
25 S. W. Rhee, A. M. Taylor, C. H. Tu, D. H. Cribbs, C. W. Cotman and N. L. Jeon, *Lab Chip*, 2005, **5**, 102–107.
26 H. J. Kim, J. W. Park, J. H. Byun, W. W. Poon, C. W. Cotman, C. C. Fowlkes and N. L. Jeon, *ACS Chem. Neurosci.*, 2012, **3**, 433–438.
27 F. M. White, in *Fluid Mechanics*, 1994, McGraw-Hill, New York, p. 333.
28 K. Haubert, T. Drier and D. Beebe, *Lab Chip*, 2006, **6**, 1548–1549.
29 Please note: Different plasma generators are built to different safety standards which differ from country to country.
30 J.-P. Frimat, H. Menne, A. Michels, S. Kittel, R. Kettler, S. Borgmann, J. Franzke and J. West, *Anal. Bioanal. Chem.*, 2009, **395**(3), 601–609.
31 R. S. Kane, S. Takayama, E. Ostuni, D. E. Ingber and G. M. Whitesides, *Biomaterials*, 1999, **20**, 2363–2376.
32 A. Folch and M. Toner, *Annu. Rev. Biomed. Eng.*, 2000, **2**, 227–256.
33 G. M. Whitesides, E. Ostuni, S. Takayama, X. Jiang and D. E. Ingber, *Annu. Rev. Biomed. Eng.*, 2001, **3**, 335–373.
34 D. Falconnet, G. Csucs, H. M. Grandin and M. Textor, *Biomaterials*, 2006, **27**, 3044–3063.
35 M. Théry, *J. Cell Sci.*, 2010, **123**, 4201–4213.

36 D. Scholz, D. Poltl, A. Genewsky, M. Wenig, T. Waldmann, S. Schildkneckt and M. Leist, *J. Neurochem.*, 2011, **119**, 957–971.
37 A. D. Lander, D. K. Fujii and L. F. Reichardt, *J. Cell Biol.*, 1985, **101**(3), 898–913.
38 C. Ionescu-Zanetti, R. M. Shaw, J. Seo, Y.-N. Jan, L. Y. Jan and L. P. Lee, *Proc. Natl. Acad. Sci. U. S. A.*, 2005, **102**(26), 9112–9117.
39 A. M. Taylor, D. C. Dieterich, H. T. Ito, S. A. Kim and E. M. Schuman, *Neuron*, 2010, **66**, 57–68.
40 L. R. Huang, E. C. Cox, R. H. Austin and J. C. Sturm, *Science*, 2004, **304**(5673), 987–990.
41 N. Li and A. Folch, *Exp. Cell Res.*, 2005, **311**(2), 307–316.
42 C. D. James, R. Davis, M. Meyer, A. Turner, S. Turner, G. Withers, L. Kam, G. Banker, H. Craighead, M. Isaacson, J. Turner and W. Shain, *IEEE Trans. Biomed. Eng.*, 2000, **47**(1), 17–21.
43 J. C. Chang, G. J. Brewer and B. C. Wheeler, *Biomed. Microdevices*, 2000, **2**(4), 245–253.
44 F. Morin, N. Nishimura, L. Griscom, B. LePioufle, H. Fujita, Y. Takamura and E. Tamiya, *Biosens. Bioelectron.*, 2006, **21**(7), 1093–1100.
45 S. B. Jun, M. R. Hynd, N. Dowell-Mesfin, K. L. Smith, J. N. Turner, W. Shain and J. S. Kim, *J. Neurosci. Methods*, 2007, **160**, 317–326.
46 S. Hosmane, I. H. Yang, A. Ruffin and N. Thakor, *Lab Chip*, 2010, **10**, 741–747.
47 J. Park, H. Koito, J. Li and A. Han, *Lab Chip*, 2012, **12**, 3296–3304.
48 I. H. Yang, D. Gary, M. Malone, S. Dria, T. Houdayer, V. Belegu, J. W. McDonald and N. Thakor, *NeuroMol. Med.*, 2012, **14**(2), 112–118.
49 W. W. Poon, M. Blurton-Jones, C. H. Tu, L. M. Feinbery, M. A. Chabrier, J. W. Harris, N. L. Jeon and C. W. Cotman, *Neurobiol. Aging*, 2011, **32**(5), 821–833.
50 S. Shoham, D. H. O'Connor, D. V. Sarkisov and S. S.-H Wang, *Nat. Methods*, 2005, **2**(11), 837–843.
51 N. Lemon and D. Manahan-Vaughan, *J. Neurosci.*, 2006, **26**(29), 7723–7729.